
VOLUME 52 NUMBER 5
SEPTEMBER 2009
ISSN 1350-4495
ELSEVIER
INFRARED PHYSICS & TECHNOLOGY
An international research journal which covers the whole field of infrared physics and technology: theory, experiment, devices and instrumentation.
Available online at www.sciencedirect.com
ScienceDirect

Infrared Physics & Technology 52 (2009) 166–173

Contents lists available at ScienceDirect

Infrared Physics & Technology

journal homepage: www.elsevier.com/locate/infrared

Analysis of point-target detection performance based on ATF and TSF

Feng Xue [a,*], Anatoly G. Yagola [b]

[a] Research Center for Space Optical Engineering, Harbin Institute of Technology, Harbin 150001, China
[b] Department of Mathematics, Faculty of Physics, Lomonosov Moscow State University, Moscow 119899, Russia

ARTICLE INFO

Article history:
Received 11 December 2008
Available online 31 July 2009

Keywords:
Point-target detection
Transition course
ATF
TSF

ABSTRACT

In many real applications such as remote sensing and space surveillance, traditional method based on ideal imaging has already been well-established. It is widely applied to analyze point-target detection performance of electro-optical imaging system, including signal-to-noise ratio (SNR) and noise equivalent temperature difference (NETD). However, this method cannot accurately predict these performance parameters, as it fails to take into account the influence of optical blurring caused by atmospheric turbulence, optics diffraction, optical aberrations, etc. In this sense, the methods, if proposed to thoroughly incorporate degrading factors into object acquisition model, would succeed to describe point-target detection performance to more degree of accuracy. The main focus of this article is to quantitatively analyze the influence of optical blurs upon point-target detection, and to establish close relationship between optical blurring and metrics of point-target acquisition. This point can be interpreted and achieved mathematically: the mathematical analysis based on image acquisition model is to combine Aperiodic Transfer Function (ATF) and Target Size Function (TSF) with analysis of SNR and NETD. In addition, the concept of NETD, traditionally used to describe extended object detection, is generalized and equivalently applied to analyze point-target detection. This refined method can be directly and conveniently used for faithfully predicting detection performance, and provides a more reliable benchmark for improving measurement setup, if we properly estimate the degree of image distortion.

1. Introduction

The basic function of electro-optical imaging system is optical collection, electro-optical conversion, electronic processing and multiplexing, image reconstruction, and display of object plane image information created by illumination or reflection of object [1–4]. The major functions are always associated with typical configuration of system. Equivalently, the actual configuration and implementation of system strongly depends on the top-level requirements and resulting flow-down system specifications [1–3,5–8]. When the system is designed for object detection, analysis of object detection performance is strongly recommended before fulfilling this task. The analysis could predict system operating performance, and provide a reliable benchmark for improving system design and choosing application environments [5–8,14–15]. The more accurate the prediction of object detection performance is; the more reliable implementation the system will have [2,3,6–8]. So it is necessary to analyze object detection performance in advance, if a system is designed to detect object in some specific situations.

Analysis of object detection performance has been developed for several decades [1–4,6], and is still a valid challenge for performance evaluation of electro-optical imaging system [1,2,9–10]. Now technologies of object detection, to most extent, rely on object acquisition model. In other words, in order to detect object that is of interest, it is often to use detector to collect flux emanating from objects and transmitting optical system, and to traditionally consider its output voltage as system response [1–3]. In spite of a large amount of literature that dedicated to object detection [1–3,9–13], it still has not been studied thoroughly due to the fact that most people consider object detection under the assumption of ideal imaging [1–3,10]. People often simply assume ideal imaging case, where the effects of any image-degradation factors during the object acquisition process are ignored [1–3,10]. In practice, when the projected area of object is much larger than that of detector, the detector is flood-illuminated so that system response is not influenced by optical blurring [1,2]. However, unlike extended object detection described above, when image size of observed object is somewhat smaller or comparable to detector size, the object cannot be resolved by system. In this case, optical blurring limits image size of object, and changes light-intensity distribution in the scope of the detector [1,2,9], shown as Fig. 1. Though Fig. 1 on sub-pixel scale cannot be displayed on screen, the distribution change will contribute to the output voltage of this pixel. As optical

* Corresponding author.
E-mail address: xuefeng2009@gmail.com (F. Xue).

1350-4495/$ - see front matter
doi:10.1016/j.infrared.2009.07.002

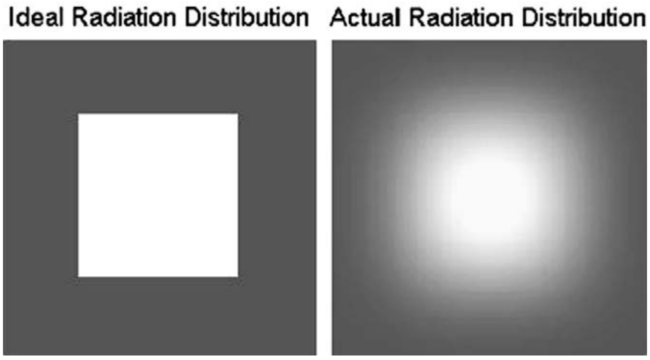

Fig. 1. Comparison between ideal and actual imaging in target pixel.

blurring reduces system response voltage, it inevitably degrades object detection performance to more or less extent, such as signal-to-noise ratio (SNR) and noise equivalent temperature difference (NETD).

In many real applications, such as remote sensing and space surveillance, observed object is at a remote distance from the imaging system. Its image size is much smaller than detector size. This limiting case is of much interest, where the system is viewing point-target [1–3,9,11–13]. In point-target detection, optical blurring must be taken into account, especially when system is operated in infrared band where optics diffraction causes more distortion to point-target image [1,2,9]. Mathematically, blurring degree is measured by optical response index, which is the only parameter of Gaussian Point Spread Function (PSF) [9], while its effect upon system response can be represented by Aperiodic Transfer Function (ATF) and Target Size Function (TSF) [1,2]. On the other hand, traditional method used to predict point-target detection performance, simply assuming ideal imaging condition without any image distortions [1–4,6–8]. Cooke and Lomheim evaluated point-target detection for remote sensor, using traditional method [3,4]. Though this method has been well-established and broadly applied in many occasions, it fails to accurately predict point-target detection performance. Therefore, in order to achieve more degree of accuracy, it would be necessary to reconsider point-target detection performance and to refine traditional method, by incorporating optical blurring into this problem. This is also a key point that to be addressed in this paper.

Historically, optical blurring and its related problems have been studied for several decades, and achieved significant success [16–24]. For instance, image acquisition model was proposed to deal with optical blurring [16–18]; nanoparticles can be localized to sub-resolution by exploiting PSF and maximum-likelihood estimation [19]; point-object detection and sub-pixel position estimation algorithm including PSF's effect was developed [20]; various deconvolution algorithms were developed to remove optical blurs [21–23]. However, there are only a few works concerning the relationship between optical blurring and point-target detection [1,2,9,24]. In Refs. [1,2], Holst used to superficially discuss this problem and advance the conceptions of ATF and TSF. Focusing on the transition course from ideal point-target to extended object, he explained the non-linear correlation between image size of object and system response. However, he did not interpret this point mathematically, and combine all factors into a unified framework. As a result, he pointed out that system signal of point-target detection can only be calculated case-by-case. Additionally, he did not relate optical blurring to detection performance. In [9], Poropat analyzed small-object range performance under PSF's influence, but he did not derive widely applicable formulas to describe it and establish a framework. In [24], the authors noticed the fact that optical obscuration would result in lost of received power by detector, when the object power center is located off-center in a detector. However, they constrained their discussions only in diffraction-limited optical system, and did not noticed that due to power spread, detector captures power less than expected in ideal imaging, even when power center is positioned at detector's center. So their result cannot be directly applied to analyze point-target detection in real situations, where optical diffraction is not the only blurring factor, and point-target imaging position cannot be controlled and predicted on sub-pixel scale.

To address this problem, as regards infrared point-target detection, this paper analyzes detection performance in a different way from traditional method, mainly focusing on quantitative analysis of the effect of blurring factors upon system response, and combination of blurring degree with detection performance. To be specific, using image acquisition model proposed by Huck [14–18], PSF is combined with system response, and thus, optical response index becomes a key parameter of ATF and TSF [1,2], finally, ATF and TSF are used to describe SNR and NETD. In this way, we propose a whole system of mathematical expressions that can be widely used to predict detection performance, and make us free from case-by-case calculation. Armed with proposed method, one can quantitatively analyze point-target detection performance under the influence of optical blurring, taking advantage of ATF and TSF.

To clearly discuss this problem, some important conceptions must be defined and clarified here. Concerning relative size of object size to detector, we discuss detection performance in two categories: transition process and limiting case. Transition process refers to the changing course from point-target to extended object, i.e. image size of object is comparable to detector size. The limiting case is point-target detection. Image size of point-target is much smaller than detector size, so it is also the limit condition of transition process, when image size of object approaches zero [1,2]. Traditional method refers to object detection analysis under the assumption of ideal imaging without any image degradations, i.e. PSF is not ignored or simply assumed to be Delta function [3,4]. Our proposed method in this paper analyzes the problem under actual imaging situation, with consideration of PSF. Observed scenario consists of object and background: object is the part of interest and to be detected, and background is another part we are not concerned with. Because image size of object is smaller than one detector, target pixel is defined as the detector capturing object radiation, and its output voltage is conventionally treated as system response [1–4]. Other pixels in the array receive only background information, so they are called background pixel for simplicity. Signal is usually defined as the output voltage difference between target pixel and background pixel [1–4]. Additionally, unlike Ref. [24], we assume image center of object is fixed at the detector center, and mainly focus on transition process.

This paper is organized as follows: in Section 2, under the assumption that PSF is of Gaussian function form, mathematical expressions of both ATF and TSF is derived, based on image acquisition model; in Section 3 and Section 4, incorporating ATF and TSF into formulism of system response, the more accurate prediction of detection performance (SNR and NETD) can be achieved in a simple way. Moreover, by comparing proposed method with traditional one, it can be easily seen that the effect of optical blurring cannot be neglected in both transition course and limiting case.

2. Formulations of ATF and TSF

2.1. Establishment of system response

To discuss the effect of optical blurring upon system response, the first step would be to derive expressions of system response, using image acquisition model [16–18].

PSF is often used to describe optical blurring and measure the degree of power spread. In practice, as typical system is concerned [1–4], PSF is usually modeled as Gaussian function [9]:

$$h_{\text{optics}}(x,y) = \pi\xi^2 \cdot \exp[-(\pi\xi)^2 \cdot (x^2 + y^2)] \tag{1}$$

where ξ called optical response index, represents the degree of optical blurring. This key parameter can be adjusted so as to make PSF model suitable for specific environment. Refs. [1,9] proposed methods how to estimate optical response index, considering all the blurring factors. In infrared object detection, typical value of ξ is 2.0–4.5 $\times$ 10^4 m^{-1} [1–4,9]. $\pi\xi^2$ is normalization coefficient of optics PSF.

Pixel is regarded as spot aperture, if it is of rectangular shape, $h_{\text{pixel}}(x, y)$ can be written as [16–18]:

$$h_{\text{pixel}}(x,y) = \text{rect}\left(\frac{x}{\Delta_x}, \frac{y}{\Delta_y}\right) = \begin{cases} 1 & |x| \le \frac{\Delta_x}{2}, \quad |y| \le \frac{\Delta_y}{2} \\ 0 & |x| > \frac{\Delta_x}{2}, \quad |y| > \frac{\Delta_y}{2} \end{cases} \tag{2}$$

where rect-function denotes rectangular function; Δ_x and Δ_y denote pixel size along x- and y-directions. This spot aperture essentially represents integration process of detector: detector collects infrared radiation and integrates irradiance over the whole detector region to radiation power.

We can take, for example, a simple input scene $f(x, y)$ on focal plane array (FPA), which contains high-frequency features:

$$f(x,y) = \frac{A_0}{\pi \cdot fl^2} M_B \cdot \text{rect}\left(\frac{x}{B_x}, \frac{y}{B_y}\right) + \frac{A_0}{\pi \cdot fl^2}(M_T - M_B) \cdot \text{rect}\left(\frac{x}{T_x}, \frac{y}{T_y}\right) \tag{3}$$

where $f(x, y)$ represents the projected version of our observed scenario that consists of object and background. This expression describes an original scene where point-target of M_T infrared irradiance is located in a wide background of uniform infrared irradiance M_B; B_x, B_y and T_x, T_y denote image size of background and object, respectively; B_x, $B_y \gg \Delta_x$, Δ_y; A_0 stands for entrance aperture area of system; fl is focal length.

Image acquisition model in [16–18] can be written as:

$$g(m,n) = K \cdot [f(x - u_x, y - u_y) * h_{\text{optics}}(x,y) * h_{\text{pixel}}(x,y)] \cdot \delta\left(\frac{x}{\Delta_x} - m, \frac{y}{\Delta_y} - n\right) \tag{4}$$

where $g(m, n)$ stands for system output voltage sequences, acquired by detector array of imaging system, each value of g corresponds to each detector's output voltage [16–18]; (m, n) is pixel index in x- and y-directions; $\delta(x, y)$ symbolizes sampling process; K is conversion ratio from radiation power to voltage [1,2]; (u_x, u_y) is sub-pixel image position of object, so-called sub-pixel shifts or phasing [1,17]. As mentioned in Section 1, we simply assume object is projected to target pixel's center, i.e. assume (u_x, u_y) to be $(0, 0)$. The output voltage of target pixel is $g(0, 0)$, which is also system response. Thus, combining Eqs. (1)–(4) and applying properties of self-defined ierf-function (see Appendix A), we obtain system response is:

$$g(T_x,T_y) = K\frac{A_0}{\pi \cdot fl^2} M_B A_d + K\frac{A_0}{\pi \cdot fl^2}(M_T - M_B)A_d \cdot \text{ierf}\left(\pi\xi\frac{T_x}{2}, \pi\xi\frac{\Delta_x}{2}\right) \cdot \text{ierf}\left(\pi\xi\frac{T_y}{2}, \pi\xi\frac{\Delta_y}{2}\right) \tag{5}$$

where A_d is detector area: $A_d = \Delta_x\Delta_y$

Without consideration of optical blurring, [1–4] suggested system response in traditional method can be written as:

$$g_{\text{ideal}}(T_x,T_y) = \begin{cases} K\frac{A_0}{\pi \cdot fl^2} M_B A_d + K\frac{A_0}{\pi \cdot fl^2}(M_T - M_B)A_T & A_T \le A_d \\ K\frac{A_0}{\pi \cdot fl^2} M_T A_d & A_T > A_d \end{cases} \tag{6}$$

where A_T is ideal imaging area of point-target: $A_T = T_xT_y$.

Considering Eq. (6), when observed object is extended one, and can be resolved by imaging system, detector is flood-illuminated by object. In this case, system response g does not infer anything about extended object other than its irradiance. Equivalently, system response g is independent of image size of extended object A_T [1,2], it depends on only detector size A_d, because basic output unit of imaging system is detector but not observed object. However, in transition process, target pixel in not full of object radiation, so image size of object contributes to system response. Thus, a simple linear relationship between A_T and system response g holds for ideal imaging [3,4]. Comparing Eq. (5) with Eq. (6), it can be found that in Eq. (5), optical blurring, denoted by ξ, has been successfully incorporated into system response g. In other words, Eq. (5) makes a quantitative connection between optical blurring and system response.

2.2. Detection signal analysis

Now we are at the position to obtain signal expression under PSF's influence, since both definitions of ATF and TSF are raised from signal analysis. Because what is of interest is the differential output of system [1,2], signal, as traditionally defined [1–4], should be output voltage difference between target pixel and background pixel, and can be written as:

$$s(T_x,T_y) = g(T_x,T_y) - g_b \tag{7}$$

where g_b is output voltage of background pixel:

$$g_b = K\frac{A_0}{\pi \cdot fl^2} M_B A_d \tag{8}$$

Therefore, combining (5)–(8), we have:

$$s(T_x,T_y) = K\frac{A_0}{\pi \cdot fl^2}(M_T - M_B)A_d \cdot \text{ierf}\left(\pi\xi\frac{T_x}{2}, \pi\xi\frac{\Delta_x}{2}\right) \cdot \text{ierf}\left(\pi\xi\frac{T_y}{2}, \pi\xi\frac{\Delta_y}{2}\right) \tag{9}$$

$$s_{\text{ideal}}(T_x,T_y) = \begin{cases} K\frac{A_0}{\pi \cdot fl^2}(M_T - M_B)A_T & A_T \le A_d \\ K\frac{A_0}{\pi \cdot fl^2}(M_T - M_B)A_d & A_T > A_d \end{cases} \tag{10}$$

Signal s shares the same explanation with system response g, and is also a pixel-based measured.

2.3. Analysis of ATF

From Eqs. (9) and (10), in transition course, maximum value of signal s is achieved, when extended object is observed, no matter what its image size exactly is. In this case, as illustrated by Eq. (10), maximum signal is independent of image size of object, and is determined only by detector size:

$$\max[s(T_x,T_y)] = K\frac{A_0}{\pi \cdot fl^2}(M_T - M_B)A_d \tag{11}$$

Aperiodic Transfer Function (ATF) is essentially normalized form of signal s: it transforms the maximum value of signal to unity [1]. So we have:

$$\text{ATF}(T_x,T_y) = \frac{s(T_x,T_y)}{\max[s(T_x,T_y)]} = \text{ierf}\left(\pi\xi\frac{T_x}{2}, \pi\xi\frac{\Delta_x}{2}\right) \cdot \text{ierf}\left(\pi\xi\frac{T_y}{2}, \pi\xi\frac{\Delta_y}{2}\right) \tag{12}$$

$$\text{ATF}_{\text{ideal}}(T_x,T_y) = \frac{s_{\text{ideal}}(T_x,T_y)}{\max[s(T_x,T_y)]} = \begin{cases} A_T/A_d & A_T \le A_d \\ 1 & A_T > A_d \end{cases} \tag{13}$$

ATF is mainly used for quantitatively describing the transition process, especially when taking into account optical blurring. This function brings great benefit to people who want to accurately predict object detection performance: once image size of object is known, signal can be calculated as multiplication of ATF by its maximum value, using Eqs. (11) and (12). Assuming pixel size A_d is $30\,\mu m \times 30\,\mu m$, Fig. 2 shows that the relationship between ATF and A_T under three situations: ideal imaging and two different degrees of optical blurring. Obviously, the more degree the optical blurring has, the smaller value ATF is. As ATF is also pixel-based measured, once object is resolved by system, ATF is independent of A_T. So ATF approaches 1 when A_T is increasing.

Conceptually, the great significance of ATF is that it finely describes the subtle relationship on sub-pixel scale, which cannot be displayed on screen. From another viewpoint, ATF is concerned with frequencies higher than cutoff frequency of system, so it cannot be shown in frequency domain. That is also the reason why this function is named as "Aperiodic".

As mentioned in Section 1, in practice, many real applications correspond to the limiting case, where imaging system is viewing ideal point-targets [3,4]. In this case that is of interest, optical blurring dominates image size of point-target and the scope of its radiation spread, which becomes independent of A_T. However, ATF fails to be used for calculating signal in the limiting case, because ATF approaches to zero. In order to quantitatively represent this limiting case, Target Size Function (TSF) would be helpful to come over this obstacle.

2.4. Analysis of TSF

TSF is defined as the ratio between actual ATF and ideal ATF, so we have:

$$\mathrm{TSF}(T_x, T_y) = \frac{\mathrm{ATF}(T_x, T_y)}{\mathrm{ATF}_{\mathrm{ideal}}(T_x, T_y)} \tag{14}$$

TSF can be used to quantify the difference of ideal with actual situation and evaluate the magnitude of optical blurring effect upon signal. The more value TSF has, the less difference between ideal and actual imaging would be, the less degree of optical blurring upon signal is. For instance, TSF = 1 means optical blurring does not affect object detection at all. From Eqs. (12)–(14), we have

$$\mathrm{TSF}(T_x, T_y) = \begin{cases} \frac{A_d}{A_T} \cdot \mathrm{ierf}\left(\pi\xi\frac{T_x}{2}, \pi\xi\frac{\Delta_x}{2}\right) \cdot \mathrm{ierf}\left(\pi\xi\frac{T_y}{2}, \pi\xi\frac{\Delta_y}{2}\right) & A_T \le A_d \\ \mathrm{ierf}\left(\pi\xi\frac{T_x}{2}, \pi\xi\frac{\Delta_x}{2}\right) \cdot \mathrm{ierf}\left(\pi\xi\frac{T_y}{2}, \pi\xi\frac{\Delta_y}{2}\right) & A_T > A_d \end{cases} \tag{15}$$

Fig. 3 shows the correlation between TSF and A_T. It illustrates two points: (1) during the transition process, TSF is minimized when A_T and A_d are identical. It means optical blurring causes most significant effect on object detection at this point and (2) the more extent of optical blurring reduces TSF.

Signal can also be written using TSF:

$$s(T_x, T_y) = \mathrm{TSF}(T_x, T_y) \cdot K \frac{A_0}{\pi \cdot fl^2}(M_T - M_B)A_T \tag{16}$$

The important benefit of TSF lies in Eq. (16), which enables us to calculate signal in limiting case of ideal point-target. As A_T approaches to zero, TSF has its limit:

$$\lim_{T_x, T_y \to 0} \mathrm{TSF}(T_x, T_y) = \mathrm{erf}\left(\pi\xi\frac{\Delta_x}{2}\right) \cdot \mathrm{erf}\left(\pi\xi\frac{\Delta_y}{2}\right) \tag{17}$$

Eq. (17) shows that in point-target detection, TSF approaches a constant that is independent of A_T. TSF depends only on the degree of optical blurring ξ and detector size A_d. This equation demonstrates that it is entirely possible to derive a widely applicable formula of TSF not as Holst stated in [1] that TSF can only be calculated on a case-by-case basis in point-target detection. For example, assuming A_d is $30\,\mu m \times 30\,\mu m$, and ξ to be $4.5 \times 10^4\ m^{-1}$ and $3.0 \times 10^4\ m^{-1}$, we can easily obtain TSF is 0.98 and 0.91, respectively.

Thus, we have established a framework, including Eqs. (11)–(17), for dealing with a wide range of various situations in object detection. As mentioned in Section 1, our discussion is constrained by the precondition that point-target is projected at detector center. Eq. (17) refers to this case, where TSF is maximized [1]. If detector size becomes relatively smaller for the sake of spatial resolution, or more blurring factors need to be considered, maximum value of TSF would still probably be smaller than one. It has been proved by the above example. Surely, if point-target image is not located at the center of target pixel, i.e. when sub-pixel shift (u_x, u_y) is not (0, 0), TSF would dramatically decrease as following:

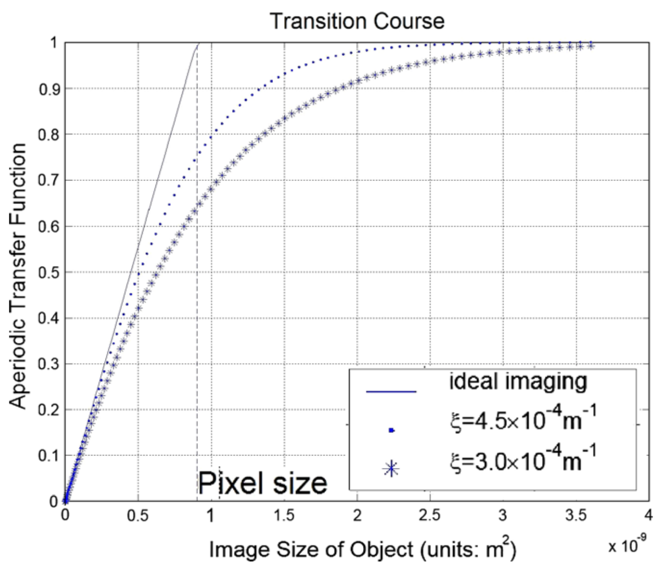

Fig. 2. Relationship between ATF and image size of object.

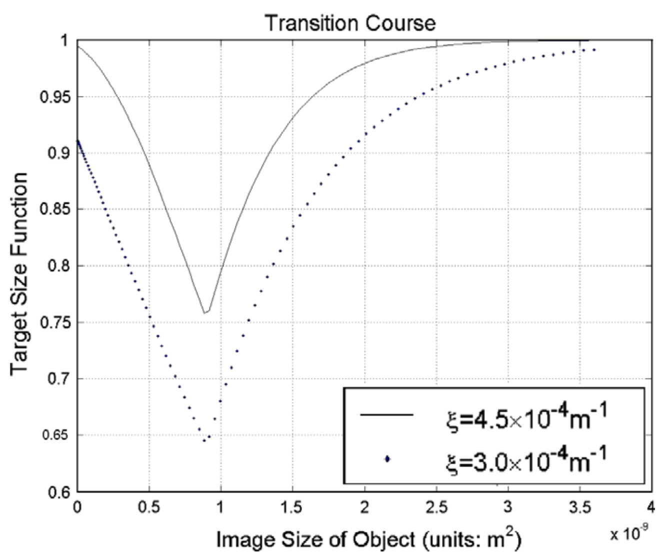

Fig. 3. TSF in transition process.

$$\lim_{T_x,T_y\to 0}\mathrm{TSF}(u_x,u_y)=\frac{1}{2}\left\{\mathrm{erf}\left[\pi\xi\left(u_x+\frac{\Delta_x}{2}\right)\right]-\mathrm{erf}\left[\pi\xi\left(u_x-\frac{\Delta_x}{2}\right)\right]\right\}\times\frac{1}{2}\left\{\mathrm{erf}\left[\pi\xi\left(u_y+\frac{\Delta_y}{2}\right)\right]-\mathrm{erf}\left[\pi\xi\left(u_y-\frac{\Delta_y}{2}\right)\right]\right\}\tag{18}$$

Eq. (18) can be obtained by replicating the derivation throughout Section 2. When point-target is exactly located between detectors, TSF reaches its minimum:

$$\min_{u_x,u_y}\lim_{T_x,T_y\to 0}\mathrm{TSF}(u_x,u_y)=\frac{1}{2}\mathrm{erf}(\pi\xi\Delta_x)\times\frac{1}{2}\mathrm{erf}(\pi\xi\Delta_y)\tag{19}$$

Considering typical setup parameters, its minimum approximately equals to 1/4.

Now, returning to the constrained discussion, from Eqs. (16) and (17), signal of detecting point-target is:

$$s(T_x,T_y)=\mathrm{erf}\left(\pi\xi\frac{\Delta_x}{2}\right)\cdot\mathrm{erf}\left(\pi\xi\frac{\Delta_y}{2}\right)\cdot K\frac{A_0}{\pi\cdot fl^2}(M_T-M_B)A_T\tag{20}$$

Thus, we can calculate signal in the limiting case, using Eq. (20). In this case, under PSF's influence, signal is positive proportional to A_T. Surprisingly, it coincides with ideal imaging situation, just with different proportional coefficients caused by optical blurring. This expression can be widely used in many real applications that satisfy limit condition. In addition, as this simple equality contains no any complicated or self-defined functions, it would be of much significance and convenience for predicting point-target detection performance in actual engineering.

3. Analysis of SNR

3.1. Formulation of SNR based on ATF and TSF

As electro-optical imaging system is concerned, SNR refers to pixel-based measure [1,2], and is traditionally defined as ratio of signal voltage to noise voltage. This definition also corresponds to Section 2.2 [1–8,11].

Usually, system noise is divided into three types: photon noise introduced by object and background radiation, detector noise and electronics noise. In practice, there is no apparent difference of system noise between ideal and actual situations. In this paper, we simply assume that optical blurring does not affect voltage level of system noise [1,2,10–11]. Here, we denote noise voltage as V_N. According to the definition, SNR is:

$$\mathrm{SNR}(T_x,T_y)=\frac{s(T_x,T_y)}{V_N}\tag{21}$$

From Eqs. (9), (10), and (21), SNR can be expressed as:

$$\mathrm{SNR}(T_x,T_y)=\frac{K\frac{A_0}{\pi\cdot fl^2}(M_T-M_B)A_d}{V_N}\cdot\mathrm{ierf}\left(\pi\xi\frac{T_x}{2},\pi\xi\frac{\Delta_x}{2}\right)\cdot\mathrm{ierf}\left(\pi\xi\frac{T_y}{2},\pi\xi\frac{\Delta_y}{2}\right)\tag{22}$$

$$\mathrm{SNR}_{\mathrm{ideal}}(T_x,T_y)=\frac{K\frac{A_0}{\pi\cdot fl^2}(M_T-M_B)A_T}{V_N}\tag{23}$$

Alternatively, SNR can be written in terms of ATF and TSF:

$$\mathrm{SNR}(T_x,T_y)=\frac{K\frac{A_0}{\pi\cdot fl^2}(M_T-M_B)A_d}{V_N}\cdot\mathrm{ATF}(T_x,T_y)\tag{24}$$

$$\mathrm{SNR}(T_x,T_y)=\mathrm{SNR}_{\mathrm{ideal}}(T_x,T_y)\cdot\mathrm{TSF}(T_x,T_y)\tag{25}$$

Thus, Eqs. (24) and (25) incorporate ATF and TSF into SNR analysis. Once optical response index ξ is estimated, ATF and TSF enable us to easily predict SNR performance in the transition process. Moreover, in the limiting case of point-target detection, SNR should be:

$$\mathrm{SNR}=\mathrm{erf}\left(\pi\xi\frac{\Delta_x}{2}\right)\cdot\mathrm{erf}\left(\pi\xi\frac{\Delta_y}{2}\right)\cdot\frac{K\frac{A_0}{\pi\cdot fl^2}(M_T-M_B)}{V_N}\cdot A_T\tag{26}$$

and

$$\mathrm{SNR}=erf\left(\pi\xi\frac{\Delta_x}{2}\right)\cdot erf\left(\pi\xi\frac{\Delta_y}{2}\right)\cdot\mathrm{SNR}_{\mathrm{ideal}}\tag{27}$$

Obviously, it is similar with signal analysis: in point-target detection, optical blurring does not break the linear relationship between SNR and A_T, just reduces its proportional coefficient.

3.2. Simulation and result

In order to show the effect of optical blurring upon SNR, we can take an example of infrared object detection: assuming that the observed scenario is described as Eq. (3) and Fig. 1; in this scenario, the temperatures of object and background are 320 K and 300 K, respectively; system typical parameters: diameter of entrance stop D_0 is 0.05 m, focal length fl is 0.1 m, transmittance of optical system is 0.8, pixel size A_d is $30\,\mu\mathrm{m}\times 30\,\mu\mathrm{m}$, responsivity R is 3×10^4 V/W, system gain G is 2×10^4, so conversion coefficient K is 6×10^8 V/W, system noise voltage V_N is 1 mV; under detection wavelength of 3–5 μm, ξ can be set as $4.5\times 10^4\,\mathrm{m}^{-1}$ or $3.0\times 10^4\,\mathrm{m}^{-1}$ to meet different environments [1,9]. We set image size of object A_T as variable. Fig. 4 shows the relationship between SNR and A_T during the transition process.

Fig. 4 illustrates that optical blurring breaks the linear relationship between SNR and A_T in the transition course. Moreover, SNR performance is measured on detector-basis: when observed object is extended, signal becomes independent of A_T. Therefore, SNR follows the same varying condition as signal and ATF: they become constants when extended object is detected, if other parameters are fixed.

In point-target detection, image size of object A_T is much smaller than detector size A_d. For simplicity, we assume A_T varying from 0 to one hundredth of A_d. It corresponds to this limiting case, shown in Fig. 5. Fig. 5 demonstrates SNR is always positive proportional to point-target imaging size, no matter whether optical blurring is considered or not. It coincides with transition course in ideal imaging shown in Fig. 4. However, optical blurring lowers the pro-

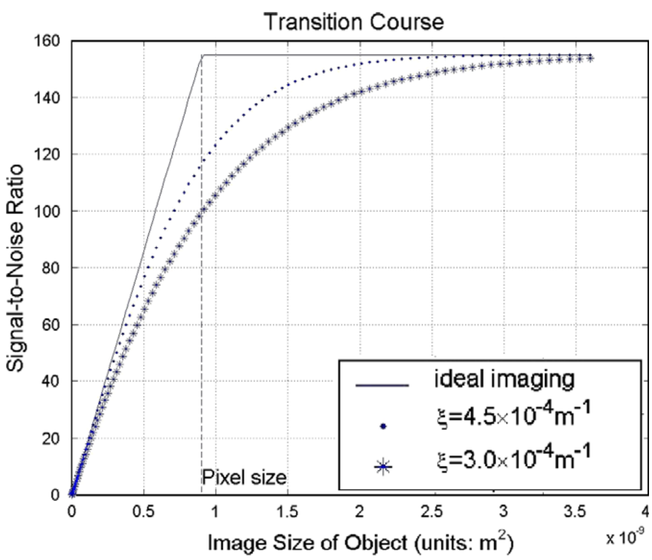

Fig. 4. SNR in transition course of image size of object.

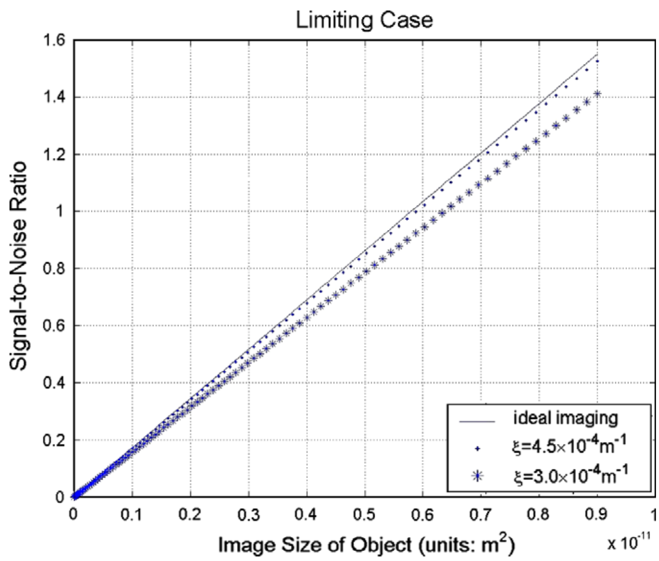

Fig. 5. SNR performance in point-target detection.

portional coefficient: the more degree optical blurring has, the smaller value the coefficient is.

4. Analysis of NETD

4.1. Different concepts of $\Delta \boldsymbol{T}$ in transition process

Traditionally, conception of NETD can only be applied to analyze extended object detection. Actually, it can also be used in describing transition process, if the notion of temperature difference ΔT is carefully specified and defined.

The first type of ΔT is apparent ΔT [1], which simply defines temperature difference of object with background, i.e.

$$\Delta T_a = T_T - T_B \tag{28}$$

The second type of ΔT is area-weighted ΔT, defined as average temperature difference of target pixel and background pixel: the former contains both point-target and background radiation, while the latter contains only background radiation [1]. Area-weighted ΔT is based on average temperature difference within the scope of pixel, and depends on relative size of A_T–A_d. Like definitions of signal and SNR, area-weighted ΔT is also measured on detector-basis. Under ideal imaging situation, area-weighted ΔT can be written as:

$$\Delta T_p = \frac{A_d T_B + A_T(T_T - T_B)}{A_d} - T_B = \frac{A_T(T_T - T_B)}{A_d} = \frac{A_T}{A_d}\cdot \Delta T_a \tag{29}$$

Obviously, area-weighted ΔT can be used more conveniently than apparent ΔT to describe transition process, since it is quantified pixel-by-pixel and obeys system working mechanism. So, can we address NETD problem in the same way to make NETD also applicable to transition process and point-target detection? The answer is positive: to describe point-target detection, we divide NETD into two types: apparent NETD and area-weighted NETD, which will be discussed as following.

4.2. Area-weighted NETD

Similarly, area-weighted NETD, denoted as NETD_p, is average temperature difference of target pixel and background pixel, which causes noise equivalent voltage of signal. We have:

$$V_N = K\frac{A_0}{\pi \cdot fl^2}[M(T_B + \mathrm{NETD}_p) - M(T_B)]\cdot A_d \tag{30}$$

NETD_p analysis has no difference with conventional method in extended object detection. NETD_p is often a tiny physical quantity, so Taylor expansion can be used to turn Eq. (30) into the following equation:

$$\mathrm{NETD}_p = \frac{V_N}{K\frac{A_0}{\pi \cdot fl^2}\cdot \frac{\partial M(T_B)}{\partial T}\cdot A_d} \tag{31}$$

Because area-weighted NETD is a pixel-based concept, it is not concerned with any optical blurring factors on sub-pixel scale. So, optical blurring does not affect area-weighted NETD as well. Due to its permanently valid for object detection, this equation can also be used to predict approximated value of apparent NETD, which will be discussed as follows.

4.3. Apparent NETD

To intuitively represent temperature difference between object and background in transition process, we propose apparent NETD, defined as temperature difference, which causes noise equivalent voltage of signal. Thus, we have:

$$V_N = K\frac{A_0}{\pi \cdot fl^2}[M(T_B + \mathrm{NETD}_a) - M(T_B)]\cdot A_d \cdot \mathrm{ATF}(T_x, T_y) \tag{32}$$

Under ideal imaging situation, we have the similar equation:

$$V_N = K\frac{A_0}{\pi \cdot fl^2}[M(T_B + \mathrm{NETD}_{\mathrm{ideal}-a}) - M(T_B)]\cdot A_d \cdot \mathrm{ATF}_{\mathrm{ideal}}(T_x, T_y) \tag{33}$$

Similarly, Eqs. (32) and (33) turns out to be:

$$\mathrm{NETD}_a = \frac{V_N}{K\frac{A_0}{\pi \cdot fl^2}\cdot \frac{\partial M(T_B)}{\partial T}\cdot A_d \cdot \mathrm{ATF}(T_x, T_y)} \tag{34}$$

$$\mathrm{NETD}_{\mathrm{ideal}-a} = \frac{V_N}{K\frac{A_0}{\pi \cdot fl^2}\cdot \frac{\partial M(T_B)}{\partial T}\cdot A_d \cdot \mathrm{ATF}_{\mathrm{ideal}}(T_x, T_y)} \tag{35}$$

Thus, we can establish relationship for two types of NETD in transition process:

$$\mathrm{NETD}_p(T_x, T_y) = \mathrm{NETD}_a \cdot \mathrm{ATF}(T_x, T_y) \tag{36}$$

To find solution to Eqs. (32) and (33), it is equivalent to solve Eq. (36). Eq. (36) provides an alternative way to calculate apparent NETD except for Eq. (34): firstly, using Eq. (31) to calculate area-weighted NETD, and then, using Eq. (36) to predict apparent NETD. Combination of Eqs. (31) and (36) would be a simple prediction of apparent NETD, though it is just an approximated value. Moreover, as area-weighted NETD is independent to A_T, Eq. (36) demonstrates that apparent NETD is inverse proportional to ATF.

Furthermore, when system is viewing an ideal point-target, ATF approaches zero. In this limiting case, Eq. (36) relying on ATF cannot be used to calculate apparent NETD. We rewrite it using TSF like this:

$$\mathrm{NETD}_p(T_x, T_y) = \mathrm{NETD}_a \cdot \frac{A_T}{A_d}\cdot \mathrm{TSF}(T_x, T_y) \tag{37}$$

Combining Eqs. (17) and (37), we have:

$$\mathrm{NETD}_p(T_x, T_y) = \mathrm{NETD}_a \cdot \frac{A_T}{A_d}\cdot erf\left(\pi\xi\frac{\Delta_x}{2}\right)\cdot erf\left(\pi\xi\frac{\Delta_y}{2}\right) \tag{38}$$

Unlike transition process illustrated by Eqs. (36) and (38) shows that in point-target detection, apparent NETD is inverse proportional to A_T, not to ATF. Therefore, this limiting case is easier to analyze than transition process.

4.4. Simulation and result

Recalling the example discussed in Section 3.2, from Eq. (31), we obtain area-weighted NETD is 138.7 mK, which is independent of A_T. Thus, we can easily calculate apparent NETD using Eq. (36). The results of transition process are shown in Fig. 6.

Fig. 6 illustrates the following three points: (1) when area-weighted NETD is fixed, apparent NETD becomes smaller when image size of object increases. And when image size of object A_T is comparable to detector size A_d, apparent NETD approaches a constant, area-weighted NETD; (2) optical blurring degrades NETD performance, and lower temperature sensitivity of system: under PSF's influence, system cannot response minor temperature fluctuations, which may be detected by the same system under ideal situation; and (3) different degrees of optical blurring causes different NETD performance: the larger value optical response index is, the worse NETD performance becomes.

Fig. 7 shows NETD performance in point-target detection calculated by Eq. (38). Since image size of point-target A_T is much smaller than detector size, apparent NETD has to be very large so that average temperature of target pixel is higher than that of background pixel by small value of area-weighted NETD. Eq. (29) also illustrates this point.

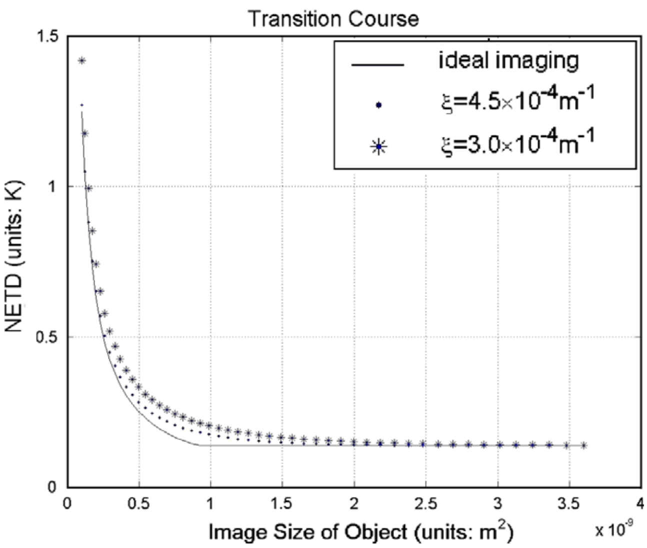

Fig. 6. Apparent NETD performance in transition course.

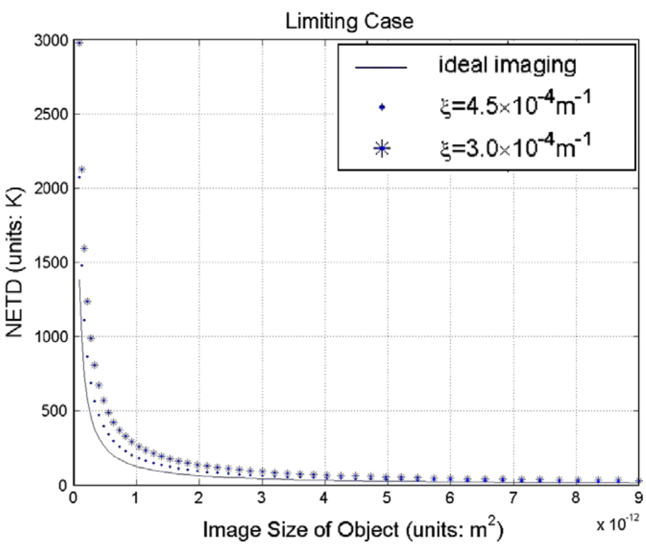

Fig. 7. Apparent NETD performance in limiting case.

5. Conclusions

This paper mainly aims at establishing mathematical connection between optical blurring and object detection performance, and enables us to more accurately analyze and predict performance in a wide range of real applications. Armed with the proposed framework, we need not to calculate detection performance case-by-case. Firstly we analyzed the transition course from point-target to extended object, using ATF and TSF, and then, to predict point-target detection by calculating limiting case of the transition process. In addition, this limiting case is essentially important, because it corresponds to most real applications when observed object is very remote to imaging system. Therefore, Eqs. (20), (26), and (38) concerning point-target detection would be very promising.

This article demonstrates that optical blurring degrades SNR and NETD performance, because it reduces signal intensity than it is expected in ideal imaging. For many real situations, this influence cannot be neglected, so our proposed method could provide more reliable prediction than traditional method.

Furthermore, our discussion reveals that in real applications, system response and signal contain lots of information on system configuration, application environment and observed object. Equivalently, the degree of optical blurring, image size of object, detector size and sub-pixel phasing contribute to system response. Therefore, it is entirely possible to estimate all the values mentioned above from output voltage of target pixel, using our established framework. It is also helpful for us to develop new algorithms of object detection and recognition.

Appendix A. Some properties of ierf(x, x_0)

To analyze ATF and TSF, it is necessary to define and specify function ierf(x, x_0) in detail. Ierf-function can be defined as:

$$ierf(x, x_0) = \frac{1}{2x_0}\int_0^x erf(t + x_0) - erf(t - x_0)dt \quad x_0 \neq 0 \tag{A1}$$

Fig. A-1 shows this function with parameter $x_0 = 2$.

Here are some properties:

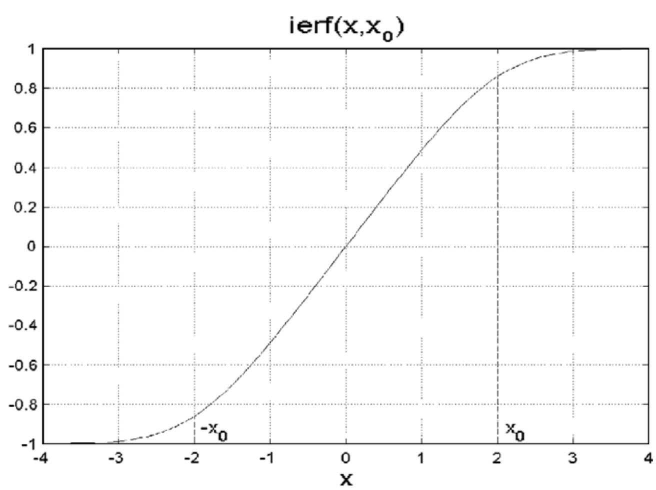

Fig. A-1. Ierf-function.

(1) ierf(x, x_0) is odd function on x. This function is defined in the interval ($-\infty$, $+\infty$), i.e.

$$ierf(x, x_0) = -ierf(-x, x_0) \tag{A2}$$

(2) The limit of ierf(x, x_0) with finite value of x_0 is:

$$\lim_{x\to+\infty} ierf(x, x_0) = 1 \tag{A3}$$

$$\lim_{x\to-\infty} ierf(x, x_0) = -1 \tag{A4}$$

References

[1] Gerald C. Holst, Electro-optical Imaging System Performance, third ed., SPIE Optical Engineering Press, Bellingham, WA, 2002.
[2] Gerald C. Holst, Testing and evaluation of infrared imaging systems, second ed., JCD Publishing and SPIE Optical Engineering Press, America, 2000 (pp. 73–80 preface to the second ed.).
[3] Bradly J. Cooke, Bryan E. Laubscher, Terrence S. Lomheim, et al., Methodology for rapid infrared multi-spectral, electro-optical imaging system performance analysis and synthesis. Proc. SPIE 2743, (1996) 52–86.
[4] Terrence S. Lomheim, Lee W. Schumann, Stanley E. Kohn, et al., Experimental characterization evaluation and diagnosis of advanced hybrid infrared focal plane array electro-optical performance, SPIE 3379 (1998) 520–554.
[5] J. Vortman, A. Bar-Lev, Dependency of thermal imaging system performance on optics and detector area, Opt. Eng. 25 (1) (1986) 123–131.
[6] Frederick A. Rosell, Predicting the performance of infrared staring arrays, SPIE 1762 (1992) 278–307.
[7] Raymond E. Hanna, Long-wave infrared hyper-spectral sensor design trade space, SPIE Proc. 4127 (2000) 157–168.
[8] J.N. Cederquist, Performance trade-offs of infrared spectral imagers, Proc. SPIE 3118 (1997) 4.
[9] George V. Poropat, Effect of system point spread function, apparent size, and detector instantaneous field of view on the infrared image contrast of small objects, Opt. Eng. 32 (10) (1993) 2598–2607.
[10] Robert L. Lucke, Robert A. Kessel, Signal-to-noise ratio, contrast-to-noise ratio, and exposure time for imaging systems with photon-limited noise, Opt. Eng. 45 (5) (2006) 132–141.
[11] Robert D. Fiete, Theodore Tantalo, Comparison of SNR image quality metrics for remote sensing systems, Opt. Eng. 40 (4) (2001) 574–585.
[12] S.L. Smith, J.A. Mooney, T.A. Tantalo, R.D. Fiete, Understanding image quality losses due to smear in high-resolution remote sensing imaging systems, Opt. Eng. 38 (5) (1999) 821–826.
[13] R.D. Fiete, Image quality and λFN/p for remote sensing systems, Opt. Eng. 38 (1999) 1229–1240.
[14] F.O. Huck, C.L. Fales, J.A. McCormick, et al., Image-gathering system design for information and fidelity, J. Opt. Soc. Am. 5 (3) (1988) 285–299.
[15] C.L. Fales, F.O. Huck, R.W. Samms, Imaging design for improved information capability, Appl. Opt. 23 (6) (1984) 872–888.
[16] F.O. Huck, N. Halyo, S.K. Park, Aliasing and blurring in 2-D sampled imagery, Appl. Opt. 19 (13) (1980) 218–224.
[17] S.K. Park, R.A. Schowengerdt, Image sampling, reconstruction, and the effect of sample-scene phasing, Appl. Opt. 21 (17) (1982).
[18] F.O. Huck, C.L. Fales, Image gathering and processing: information and fidelity, J. Opt. Soc. Am. 2 (10) (1985) 1644–1666.
[19] Francois Aguet, Dimitri Van De Ville, Michael Unser, A maximum-likelihood formalism for sub-resolution axial localization of fluorescent nanoparticles, Opt. Express. 13 (26) (2005) 10503–10522.
[20] Vincent Samson, Frédéric Champagnat, Point detection and subpixel position estimation in optical imagery, Appl. Opt. 43 (2) (2004) 257–263.
[21] J. Markham, J. Conchello, Parametric blind deconvolution: a robust method for the simultaneous estimation of image and blur, J. Opt. Soc. Am. A 16 (10) (1999) 2377–2391.
[22] Pinaki Sarder, Arye Nehorai, Deconvolution methods for 3-D fluorescence microscopy images, IEEE Signal Proc. Mag. (2006) 32–45.
[23] Sudhakar Prasad, Statistical-information-based performance criteria for Richardson-Lucy image deblurring, J. Opt. Soc. Am. A 19 (7) (2002) 1286–1296.
[24] Louis M. Beyer, S.H. Cobb, Lavern C. Clune, Ensqured power for obscured circular pupils with off-enter imaging, Appl. Opt. 30 (25) (1991) 3569–3574.